現在までに、HCV の宿主細胞への侵入に関して、CD81、Scavenger receptor class B type I (SR-BI)、claudin-1 が感染受容体として機能していることが報告されている。最近、新たな HCV 感染受容体として occludin が同定され、宿主細胞への感染機構が明らかになりつつある。しかしながら、これら感染受容体の膜蛋白質は精製が難しく、また抗原性が低いことから、HCV 感染におけるこれら受容体の機能解析や受容体間の相互作用などの解明は遅々として進展していないのが現状である。

近年、出芽バキュロウイルス（BV）が目的膜蛋白質をウイルス膜上に立体構造・機能を保持したまま高効率に提示可能であることを東大先端研の浜窪隆雄博士らが見出した。出芽型 BV を用いた本方法では、精製が困難である膜蛋白質の機能解析が可能となり、更に複合体を形成する一連の膜蛋白質の機能解析にも応用できることが分かっている。これらの利点から、出芽型 BV 発現系は複数の受容体を介して感染する HCV の受容体機能解析において非常に適した解析ツールであるといえる。

以上を踏まえ、本研究では、HCV 感染において主要な役割を担っている 4 受容体の単独、もしくは複合での生化学的解析を行うため、出芽 BV 発現系を利用した解析を行うこととした。平成 21 年度は、HCV 感染機構の解析に先立って、ウイルス感染機構が明らかとなっている 5 型アデノウイルス感染機構をモデル系として利用し、感染受容体提示 BV がウイルス感染機構の解析に応用可能であることを確認し CD81 提示 BV、SR-BI 提示 BV、claudin-1 提示 BV および occludin 提示 BV の作製に成功した。平成 22 年度に、single HCV 受容体提示 BV の HCV 感染阻害活性を解析したところ、いずれの HCV 受容体提示 BV でも感染阻害効果は観察されなかった。

本年度は、複数の HCV 受容体提示 BV を作製し、HCV 感染阻害活性を解析した。

B. 研究方法

B.1. 複数の HCV 感染受容体提示 BV の作製および精製

HCV 感染受容体である CD81、SR-BI、claudin-1 または occludin 遺伝子を搭載したトランスファーベクター、pFastBac-CD81、pFastBac-SR-BI 、 pFastBac-claudin-1 、pFastBac-occludin を用いて各感染受容体発現 bacmid を以下の方法により作製した。

トランスファーベクターを *E. coli* DH10Bac (Invitrogen 社) にトランスフォーメーションし、IPTG, X-gal 含有 TGK plate で培養し、bacmid DNA を回収した。Bacmid への HCV 感染受容体遺伝子の挿入は以下のプロトコールに準じ、PCR 法により確認した。上述した bacmid 溶液 (0.1 mg/mL) 1 μL、10 x LA PCR buffer 2 μL、25 mM $MgCl_2$ 2 μL、2.5 mM dNTP mix 3.2 μL、10 μM primers 1 μL、滅菌精製水 9.6 μL、5 U/μL Takara LA taq 0.2 μL を混合し、forward プライマー（:5′-TGTAAAACGACGGCCAGT -3′)、reverse プライマー (5′- GGAAACAGCTATGACCATG -3′) を使用した。PCR 反応は、94 ℃ 2 min の後、94 ℃ 30 sec, 55 ℃ 30 sec、68 ℃ 4 min を 35 サイクルにて行った。PCR 産物を電気泳動し目的遺伝子の挿入を確認後、当該 bacmid DNA を DH5α にトランスフォーメーションし、IPTG, X-gal 含有 TGK plate で培養、白色独立大腸菌クローンをスモールスケール培養し、HCV 感染受容体発現 bacmid DNA を得た。尚、wild type-BV （WT-BV）作製用の bacmid は青色独立大腸菌クローンから精製し、同様

の条件で PCR を行い組換えが起きていないことを確認したものを使用した。

トランスフェクション試薬 Cellfectin（Invitrogen 社）を用いて bacmid DNA を Sf9 細胞に形質導入した。3 日間培養後、培養上清（低タイターBV）を回収し、新たに用意した Sf9 細胞に感染させ、BV の増幅を行った。感染 2 日後の培養液を 800 g、10 分間遠心し、高タイターBV を回収し、4 ℃にて保存した。得られた高タイター BV は BacPAK™ Baculovirus Rapid Titer Kit（Clontech 社）を用いてタイターを測定した。

4 受容体提示 BV（4R-BV: CD81、SR-BI、claudin-1、occludin 提示 BV）、3 受容体提示 BV（3R-BV: CD81、claudin-1、occludin 提示 BV）および 2 受容体提示 BV（2R-BV: CD81、occludin 提示 BV）は、高タイターBV をそれぞれ multiplicity of infection （MOI）2.5 で Sf9 細胞に共感染させ、3 日間培養することにより作製した。感染 3 日後の培養上清を 800 g、10 分間遠心し、上清を回収した。上清 18400 rpm、25 分間、4 ℃で遠心後上清を除去した。沈澱に PBS を添加し再懸濁後、800 g、10 分間遠心し、沈澱した不純物を除去した。当該上清を 18400 rpm、25 分間遠心し、BV を沈澱させた。沈澱を 1%プロテアーゼ阻害剤（SIGMA 社）を含む TBS により再懸濁、800 g、10 分間遠心した。本上清画分を精製 BV とした。実験では、精製 BV の蛋白量を BCA protein assay kit （Thermo 社）により測定した値を基に添加濃度を設定した。精製した BV は 4℃にて保存した。尚、wild-BV も上記と同様のプロトコールにて作製した。

B.2. HCV 感染受容体提示 BV の発現確認

精製した HCV 感染受容体提示 BV を lysis buffer（20 mM Tris-HCl, 150 mM NaCl, 1% TritonX, 1% protease inhibitor）を用いて可溶化し、14000 rpm、5 分間遠心後、上清を回収した。Pierce BCA™ Protein Assay Kit を用いて上清のタンパク定量を行った。上清を 1 mg/mL となるように SDS サンプルバッファー[62.5 mM Tris-HCl (pH6.8), 5% 2-mercaptoethanol, 2% SDS, 10% glycerol, 0.002% bromophenol blue]で調製し、100℃, 5 分間処理後、14000 rpm、5 分間遠心した上清を SDS-PAGE 後、Immobilon-P Transfer Membrane（Millipore 社）に泳動産物を転写した。本メンブレンを 5%スキムミルクでブロッキングし、1 次抗体、2 時間、ペルオキシダーゼ標識 2 次抗体、1 時間反応させた。ECL Western blotting detection system（GE Healthcare 社）を用いて目的とするタンパク質バンドの検出を行った。

CD81 の検出には mouse anti-human CD81 抗体（BD Biosciences 社）および peroxidase conjugated goat anti-mouse IgG（Millipore 社）、SR-BI の検出には peroxidase conjugated SR-BI antibody（Novus Biologicals 社）、claudin-1 の検出には rabbit anti-claudin-1 抗体（ZYMED 社）および peroxidase conjugated goat anti-rabbit IgG（Millipore 社）、occludin の検出には mouse anti-occludin 抗体（ZYMED 社）および peroxidase conjugated goat anti-mouse IgG を使用した。

B.3. VSVpv の作製

293T 細胞を 100 mm^2 dish に播種 24 時間後、TransIT-LT1（Mirus 社）を用いて VSV G タンパク質発現プラスミド pCAG-VSVG をトランスフェクションした。プラスミド導入 24 時間後に、エンベロープ G タンパク質をルシフェラーゼ遺伝子に置き換えた VSVpv（大阪大学微生物病研究所、松浦博士より御供与頂いた）を感染させた。感染 24-36 時間後、培養液を回収し、2000 rpm、5 分間遠心した後の

上清を実験に供した。尚、VSVpv は-80 ℃にて保存した。

B.4. HCVpv の作製

293T 細胞を 100 mm^2 dish に播種し 24 時間培養した後に、TransIT-LT1（Mirus 社）を用いて HCV E1、E2 発現プラスミド pCAG-Con1 をトランスフェクションした。プラスミド導入 24 時間後、VSVpv を 2 時間作用させた後に、細胞を DMEM 8 mL で 5 回洗浄し、DMEM 10 mL を添加した。VSVpv 感染 24 時間後に培養液を回収、2000 rpm、5 分間遠心した後の上清を実験に供した。尚、HCVpv は-80 ℃にて保存した。

B.5. 侵入実験

Huh 7 細胞を 96 well plate 2×10^4 cells /well で播種し、24 時間培養した。HCVpv、VSVpv、BV、抗 gp64 抗体（Santa cruz biotechnology 社、BV の哺乳類細胞への侵入を阻害する抗体）を室温で 2 時間作用させた。培養液を除去し、上記混合液を細胞に 50 μL/well で添加し、37 ℃、30 分間または 4℃、30 分間作用後、培地を交換した。24 時間培養後、Luciferase Assay Systems（Promega 社）を用いてルシフェラーゼ活性を測定し、HCVpv、VSVpv の感染効率を評価した。

C. 研究結果

研究結果は D 項に併せて記載した。

D. 考　察

現在のところ、HCV 感染に関与する受容体として、CD81、SR-BI、claudin-1、occludin が同定されている。平成 22 年度に HCV 感染受容体提示 BV を作製し、HCVpv を用いて感染阻害活性を解析したところ、いずれの BV でも HCVpv の侵入阻害は観察されなかったことから、複数の感染受容体が HCV の細胞内侵入に関与している可能性が示唆された。

そこで本年度は、複数の感染受容体を提示させた BV を作製し、HCV 侵入阻害活性の解析を試みた。これまでの HCV 感染受容体に関する抗体、阻害剤、siRNA などを用いた研究報告を踏まえ、感染への関与が最も高いと予想される CD81 を中心に解析を進めることとした。CD81-BV、SR-BI-BV、claudin-1-BV、occludin-BV の高タイターBV 作製し、それぞれの混合液を Sf9 細胞に共感染させることで複数受容体提示 BV を作製した。2 受容体提示 BV（2R-BV：CD81、occludin 提示 BV）、3 受容体提示 BV（3R-BV：CD81、claudin-1、occludin 提示 BV）、4 受容体提示 BV（4R-BV：CD81、SR-BI、claudin-1、occludin 提示 BV）を作製し、SDS-PAGE およびウェスタンブロット法にて解析し、各 BV の作製を確認した（Fig. 1）。

次に、作製した複数受容体提示 BV を competitor として用いることで HCV 侵入における影響を解析した。HCV の侵入過程は、感染受容体との結合ステップ、エンドサイトーシスによる取り込みステップ、そしてエンドソームから細胞質への放出ステップに大別される。感染受容体は、結合ステップもしくはエンドサイトーシスステップに関与していると考えられており、4℃で作用させることで結合ステップを特異的に観察することができ、37℃の作用条件では結合とエンドサイトーシスを両方とも解析することができる条件となる。

HCVpv と複数受容体提示 BV を室温で 2 時間反応させた後に、37℃、30 分間 Huh7 細胞に作用させたところ、いずれの複数受容体提示 BV 作用群においても BV 添加量依存的な HCVpv 感染促進が観察された（Fig. 2A）。このとき、VSVpv では感染促進作用は認められなかった（Fig. 2A）。また、4℃、30 分間 Huh7 細胞に作用させた場合でも、37℃作用

の場合と同様の傾向が観察され、BV 添加量依存的に HCVpv の感染促進が認められた（Fig. 2B）。

これらの結果は、HCVpv と BV が相互作用することで結果的に HCVpv の細胞内侵入を促進していることを示唆している。このような現象はアデノウイルスおよびアデノウイルス感染受容体提示 BV を用いた解析では観察されなかったことから、HCV 感染に特異的に観察される現象である可能性がある。

感染受容体 CD81 は HCV エンベロープ E2 と直接結合することが報告されているが、本研究グループが行った BV を用いた感染実験では CD81 の関与を示唆する結果は得られていない。BV は昆虫細胞を用いて作製されるため、BV 膜上に発現しているタンパク質も昆虫細胞由来となる。哺乳類細胞と昆虫細胞ではタンパク質翻訳後の糖鎖修飾が一部異なることから、HCV エンベロープと BV 膜上の HCV 感染受容体との相互作用がヒト肝細胞での状況を反映できていない可能性も十分に考えられることから、哺乳類細胞と同様の糖鎖修飾がなされる BV 作製システムを利用した検討を実施する必要があると考えられる。

E. 結論

昨年度に引き続き、本年度も、BV を利用した膜蛋白質発現システムを用いて、HCV 感染機構に関する生化学的解析を試みた。

昨年度、CD81、SR-BI、claudin-1、occludin を提示した BV を用いて、HCVpv の感染を解析したところ、いずれの BV 処理でも HCVpv の感染は阻害されなかった。そこで本年度は、文献情報を基に HCV 感染への寄与率が高いと予想された CD81 に焦点を絞り、2～4 種類の HCV 受容体を提示した BV の作製を試み、各感染受容体提示 BV について高タイターBV を調整、共感染させることで 2～4 種類の HCV 受容体を提示した BV の作製に成功した。しかしながら、感染阻害活性を解析したところ、予想に反して 4 受容体提示 BV を含めた全ての BV 処理で HCVpv の感染阻害は観察されず、いずれの BV 処理でも HCVpv の侵入促進効果が認められた。Sf9 細胞は昆虫細胞であることから、糖鎖修飾がヒト細胞と異なる可能性があり、今後ヒト細胞の糖修飾をミミックした改良型 Sf9 細胞を用いた BV 作製を実施する予定である。

また昨今、HCV 解析細胞として注目されているヒト iPS 細胞を用いた HCV 感染機構の解析のパイロットスタデイに着手した。HCV 感染受容体 mRNA 発現を解析したところ、ヒト iPS 細胞では CD81 および occludin の mRNA、ヒト iPS 細胞由来肝様細胞では CD81、SR-BI、claudin-1、occludin の mRNA が発現していた。HCVpv はヒト iPS 細胞には感染せず、ヒト iPS 細胞由来肝様細胞に感染していた（data not shown）。これまでの HCV 感染受容体発現の確認は mRNA レベルであったことから、今後はタンパク質の細胞内局在の解析を実施することで HCV 感染機構に関する情報の集積を図りたい。

F. 健康危険情報

該当事項なし

G. 研究発表

G-1 論文発表

Isoda K, Hasezaki T, Kondoh M, Tsutsumi Y and Yagi K (2011) Effect of surface charge on nano-sized silica particles-induced liver injury. *Pharmazie* **66**(4):278-281.

Hasezaki T, Isoda K, Kondoh M, Tsutsumi Y and Yagi K (2011) Hepatotoxicity of silica nanoparticles with a diameter of 100 nm. *Pharmazie* **66**(9):698-703.

Yoshida T, Kondoh M, Ojima M, Mizuguchi H, Yamagishi Y, Sakamoto N and Yagi K (2011) Adenovirus vector-mediated assay system for hepatitis C virus replication. *Nucleic Acids Res* **39**(10):e64.

Yoshida T, Takayama K, Kondoh M, Sakurai F, Tani H, Sakamoto N, Matsuura Y, Mizuguchi H and Yagi K (2011) Use of human hepatocyte-like cells derived from induced pluripotent stem cells as a model for hepatocytes in hepatitis C virus infection. *Biochem Biophys Res Commun* **416**(1-2):119-124.

Li X, Kondoh M, Watari A, Hasezaki T, Isoda K, Tsutsumi Y and Yagi K (2011) Effect of 70-nm silica particles on the toxicity of acetaminophen, tetracycline, trazodone, and 5-aminosalicylic acid in mice. *Pharmazie* **66**(4):282-286.

Takahashi A, Kondoh M, Kodaka M and Yagi K (2011) Peptides as tight junction modulators. *Curr Pharm Des* **17**(25):2699-2703.

Yoshida T, Kondoh M and Yagi K (2011) Promising targets for anti-hepatitis C virus agents. *Curr Med Chem* **18**(8):1239-1244.

Kondoh M, Takahashi A and Yagi K (2012) Spiral progression in the development of absorption enhancers based on the biology of tight junctions. *Adv Drug Deliv Rev* **64**:515-522.

Sakurai F, Furukawa N, Higuchi M, Okamoto S, Ono K, Yoshida T, Kondoh M, Yagi K, Sakamoto N, Katayama K and Mizuguchi H (2012) Suppression of hepatitis C virus replicon by adenovirus vector-mediated expression of tough decoy RNA against miR-122a. *Virus Res* **165**:214-218.

G-2 学会発表

吉田 孟史、佐藤 芙美、渡利 彰浩、近藤 昌夫、水口 裕之、八木 清仁、RNA ポリメラーゼ I 発現系を利用した長鎖 RNA 発現ベクターの開発、第 27 回日本 DDS 学会、平成 23 年 6 月 9-10 日、東京

各務洋平、高橋梓、山浦利章、松久幸司、近藤昌夫、浜窪隆雄、八木清仁、Claudin 欠損マウスを利用した claudin binder 創製系の確立、第 27 回日本 DDS 学会、平成 23 年 6 月 9-10 日、東京

近藤昌夫、八木清仁、上皮細胞バリアの分子基盤を標的とした創薬研究の新展開、アスビオファーマ株式会社社内セミナー、平成 23 年 8 月 22 日、神戸（招待講演）

髙橋梓、斉藤郁美子、近藤昌夫、八木清仁、Claudin を標的とした非侵襲性投与技術の開発、第 61 回日本薬学会近畿支部総会・大会、平成 23 年 10 月 22 日、神戸

Yohei Kakamu, Kyohei Matsushita, Yumiko Saito, Azusa Takahashi, Koji Matsuhisa, Akihiro Watari, Masuo Kondoh, Kiyohito Yagi Azusa Takahashi, Masuo Kondoh, Hideki Kakutani, Toshiko Sakihama, Takao Hamakubo, Akihiro Watari, Kiyohito Yagi, Biochemical analysis of a novel dual claudin binder. Experimental Biology 2011, Apr 4-13, Washington, DC, USA

Kiyohito Yagi, Seiji Yamane, Hidehiko Suzuki, Akihiro Watari, Masuo Kondoh, Hiroshi Uchida, Development of novel claudin-4 binder and its application in mucosal vaccine. Experimental Biology 2011, Apr 4-13, Washington, DC, USA

Miki Kodaka, Azusa Takahashi, Toshiaki Yamaura, Yohei Kakamu, Koji Matsuhisa, Kyohei Matsushita, Akihiro Watari, Masuo Kondoh, Kiyohito Yagi, A simple screening system for claudin binders using an scFv library derived from claudin-immunized mice. Experimental Biology 2011, Apr 4-13, Washington, DC, USA

Masuo Kondoh, Yoshiaki Yamagishi, Takeshi Yoshida, Hiroyuki Mizuguchi, Naoya Sakamoto, Akihiro Watari, Kiyohito Yagi, Development of RNA pol-driven adenovirus vector expressing hepatitis C virus replicon. Experimental Biology 2011, Apr 4-13, Washington, DC, USA

Koji Matsuhisa, Azusa Takahashi, Yohei Kakamu, Miki Kodaka, Akihiro Watari, Masuo Kondoh, Kiyohito Yagi, Development of a novel claudin binder using baculoviral display for its application in mucosal absorption of drugs. 38th annual meeting & exposition of the Controlled Release Society, July 30-Aug 3, 2011, National Harbor, MA, USA.

Takeshi Yoshida, Fumi Satoh, Akihito Watari, Masuo Kondoh, Hiroyuki Mizuguchi, Naoya Sakamoto, Kiyohito Yagi, Development of an RNA polymerase I-driven adenoviral vector and its application in an HCV replication assay. 18th International Symposium of hepatitis C virus and related viruses, Sep8-12, 2011, Seattle, WA, USA.

H. 知的財産権の出願・登録状況

H-1 特許取得

該当事項なし

H-2 実用新案登録

該当事項なし

H-3 その他

該当事項なし

I. 研究協力者

鈴木英彦

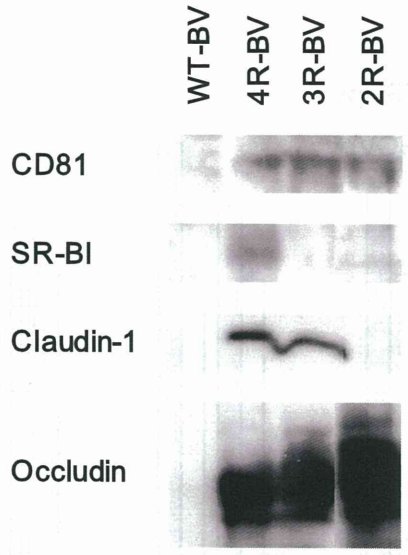

Figure 1 HCV receptor –expressing BVs.
BVs were subjected to SDS-PAGE followed by western blotting. WT-BV, wild type-BV; 4R-BV, CD81, SR-BI, claudin-1 and occludin-expressing BV; 3R-BV, CD81, claudin-1 and occludin-expressing BV; 2R-BV, CD81 and occludin-expressing BV.

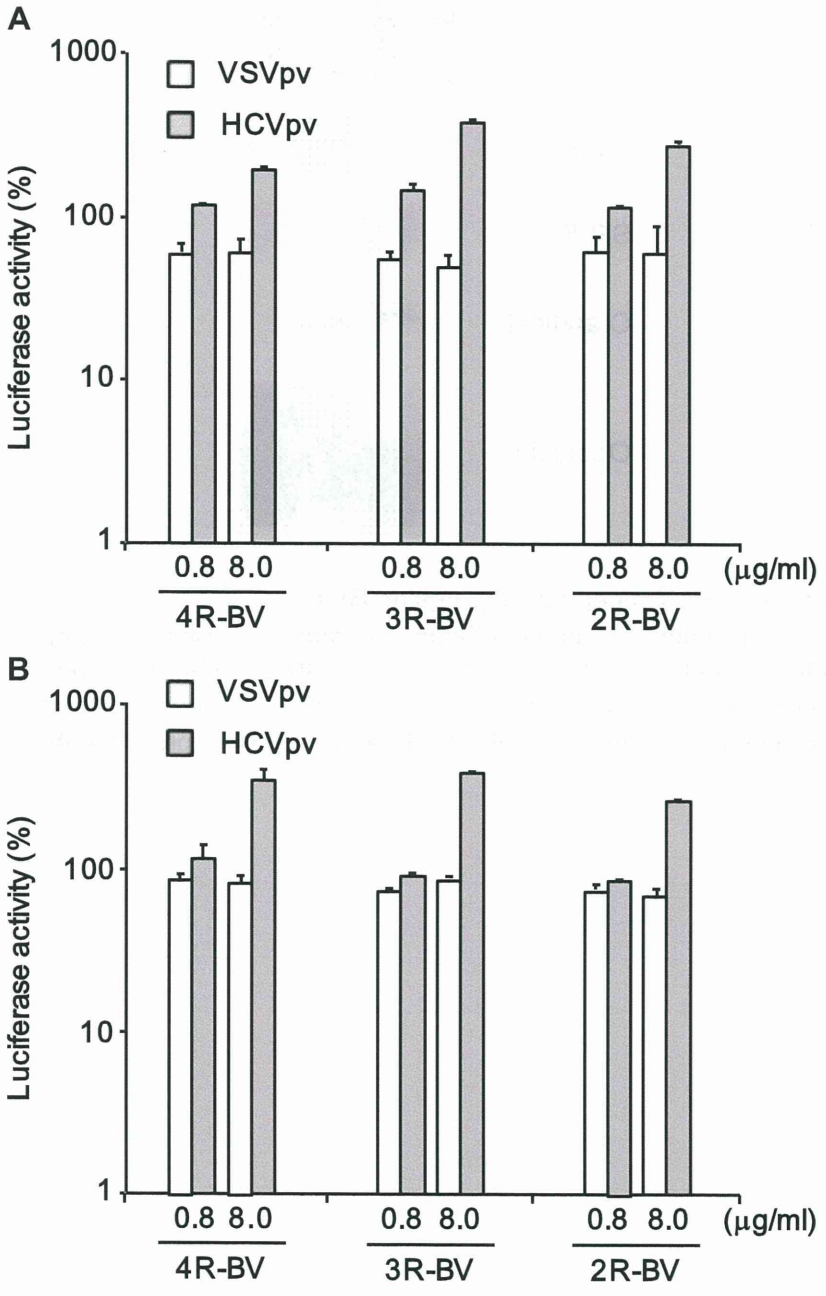

Figure 2 Effects of HCV receptors-expressing BVs on infection of HCVpv to Huh7 cells. After 30 min incubation of BVs with VSVpv or HCVpv at 37 °C (A) and 4°C (B), Huh7 cells were treated with the mixture of BVs and HCVpv for 24 h. The cells were lysed, and the luciferase activity was measured. Data are means ± SD (n = 3).

研究成果の刊行に関する一覧表

書籍

著者氏名	論文タイトル名	書籍全体の編集者名	書　籍　名	出版社名	出版地	出版年	ページ
	該当事項なし						

雑誌

発表者氏名	論文タイトル名	発表誌名	巻号	ページ	出版年
Abe Y Yoshikawa T Inoue M Nomura T Furuya T Yamashita T Nagano K Nabeshi H Yoshioka Y Mukai Y Nakagawa S Kamada H Tsutsumi Y Tsunoda S	Fine tuning of receptor-selectivity for tumor necrosis factor-α using a phage display system with one-step competitive panning	*Biomaterials*	32	5498-5504	2011
Isoda K Hasezaki T Kondoh M Tsutsumi Y Yagi K	Effect of surface charge on nano-sized silica particles-induced liver injury	*Pharmazie*	66	278-281	2011
Hasezaki T Isoda K Kondoh M Tsutsumi Y Yagi K	Hepatotoxicity of silica nanoparticles with a diameter of 100 nm	*Pharmazie*	66	698-703	2011
Yoshida T Kondoh M Ojima M Mizuguchi H Yamagishi Y Sakamoto N Yagi K	Adenovirus vector-mediated assay system for Hepatitis C virus replication	*Nucleic Acid Res*	39	E64	2011
Yoshida T Takayama K Kondoh M Sakurai F Tani H Sakamoto N Matsuura Y Mizuguchi H Yagi K	Use of human hepatocyte-like cells derived from induced pluripotent stem cells as a model for hepatocytes in hepatitis C virus infection	*Biochem Biophys Res Commun*	416	119-124	2011

Li X Kondoh M Watari A Hasezaki T Isoda K Tsutsumi Y Yagi K	Effect of 70-nm silica particles on the toxicity of acetaminophen, tetracycline, trazodone, and 5-aminosalicylic acid in mice.	*Pharmazie*	66	282-286	2011
Takahashi A Kondoh M Suzuki H Yagi K	Claudin as a target for drug development	*Curr Med Chem*	18	1861-1865	2011
Yoshida T Kondoh M Yagi K	Promising targets for anti-hepatitis C virus agents	*Curr Med Chem*	18	1239-1244	2011
Kondoh M Takahashi A Yagi K	Spiral progression in the development of absorption enhancers based on the biology of tight junctions	*Adv Drug Deliv Rev*	64	515-522	2012
Sakurai F Furukawa N Higuchi M Okamoto S Ono K Yoshida T Kondoh M Yagi K Sakamoto N Katayama K Mizuguchi H	Suppression of hepatitis C virus replicon by adenovirus vector-mediated expression of tough decoy RNA against miR-122a	*Virus Res*	165	214-218	2012

Biomaterials 32 (2011) 5498–5504

Contents lists available at ScienceDirect

Biomaterials

journal homepage: www.elsevier.com/locate/biomaterials

Fine tuning of receptor-selectivity for tumor necrosis factor-α using a phage display system with one-step competitive panning

Yasuhiro Abe [a], Tomoaki Yoshikawa [a,b], Masaki Inoue [a], Tetsuya Nomura [a], Takeshi Furuya [a,b], Takuya Yamashita [a,b], Kazuya Nagano [a], Hiromi Nabeshi [a,b], Yasuo Yoshioka [a,c], Yohei Mukai [a,b], Shinsaku Nakagawa [b,c], Haruhiko Kamada [a,c], Yasuo Tsutsumi [a,b,c], Shin-ichi Tsunoda [a,b,c,*]

[a] Laboratory of Biopharmaceutical Research, National Institute of Biomedical Innovation, 7-6-8 Saito-Asagi, Ibaraki, Osaka 567-0085, Japan
[b] Graduate School of Pharmaceutical Sciences, Osaka University, 1-6 Yamadaoka, Suita, Osaka 565-0871, Japan
[c] The Center of Advanced Medical Engineering and informatics, Osaka University, 1-6 Yamadaoka, Suita, Osaka 565-0871, Japan

ARTICLE INFO

Article history:
Received 24 March 2011
Accepted 5 April 2011
Available online 5 May 2011

Keywords:
Cytokine
Molecular biology
Protein
Affinity
Bioactivity

ABSTRACT

Tumor necrosis factor-α (TNF) is one of the attractive targets for the development of anti-inflammatory and anti-tumor drugs, because it is an important mediator in the pathogenesis of several inflammatory diseases and tumor progression. Thus, there is an increasing need to understand the TNF receptor (TNFR1 and TNFR2) biology for the development of TNFR-selective drugs. Nonetheless, the role of TNFRs, especially that of TNFR2, remains poorly understood. Here, using a unique competitive panning, we optimized our phage display-based screening technique for isolating receptor-selective TNF mutants, and identified several TNFR2-specific TNF mutants with high TNFR2 affinity and full bioactivity via TNFR2. Among these mutants, the R2-7 clone revealed very high TNFR2-selectivity (1.8×10^5 fold higher than that for the wild-type TNF), which is so far highest among the reported TNFR2-selective TNF mutants. Because of its high TNFR2-selectivity and full bioactivity, the TNF mutant R2-7 would not only help in elucidating the functional role of TNFR2 but would also help in understanding the structure-function relationship of TNF/TNFR2. In summary, our one-step competitive panning system is a simple, useful and effective technology for isolating receptor-selective mutant proteins.

1. Introduction

Tumor necrosis factor-α (TNF) is a major inflammatory cytokine that plays a central role in host defense and inflammation via two receptor subtypes, TNF receptor (TNFR)1 and TNFR2 [1,2]. Elevated serum levels of TNF correlates with the severity and progression of the inflammatory diseases such as rheumatoid arthritis (RA), inflammatory bowel disease, septic shock, multiple sclerosis and hepatitis [3–5]. Currently, TNF-neutralization therapies have proven successful for the treatment of RA [4,6,7]. However, these therapies can cause serious side effects, such as tuberculosis, because TNF-dependent host defense functions are also inhibited [8,9]. Therefore, understanding the function of TNF/TNFRs is important for optimal therapy of various TNF-related autoimmune diseases. TNFR1 is constitutively expressed in most tissues and seems to be the key mediator of TNF signaling [10,11]. In contrast, the expression of TNFR2 is more restricted and is found mainly on certain T-cell subpopulations [12], endothelial cells, cardiac myocytes [13] and neuronal tissue [14,15]. Recent studies suggested that TNFR2 signaling is associated with T-cell survival [16], cardioprotection [17,18], remyelination [19], and survival of some neuron subtypes [20,21]. Although the two TNFRs have been shown to have distinct functions in some cells [22], the physiological significance of the presence of both receptors is not fully understood. Especially TNFR2-induced signaling remains elusive and need further investigation.

In order to understand the mechanism of TNFRs, we have investigated the relationship between the biological activities and structural properties of a large number of TNF mutants by phage-display technique [23,24]. However, screening efficiency of isolating TNFR2-selective TNF mutants using this technique is extremely low, and it is difficult to prepare large repertoire of TNFR2-selective TNF mutants for the structure-activity relationship study. In our previous study, we screened 500 phage clones

* Corresponding author. Laboratory of Biopharmaceutical Research, National Institute of Biomedical Innovation, 7-6-8 Saito-Asagi, Ibaraki, Osaka 567-0085, Japan. Tel.: +81 72 641 9814; fax: +81 72 6419817.
E-mail address: tsunoda@nibio.go.jp (S.-i. Tsunoda).

0142-9612/$ – see front matter © 2011 Elsevier Ltd. All rights reserved.
doi:10.1016/j.biomaterials.2011.04.018

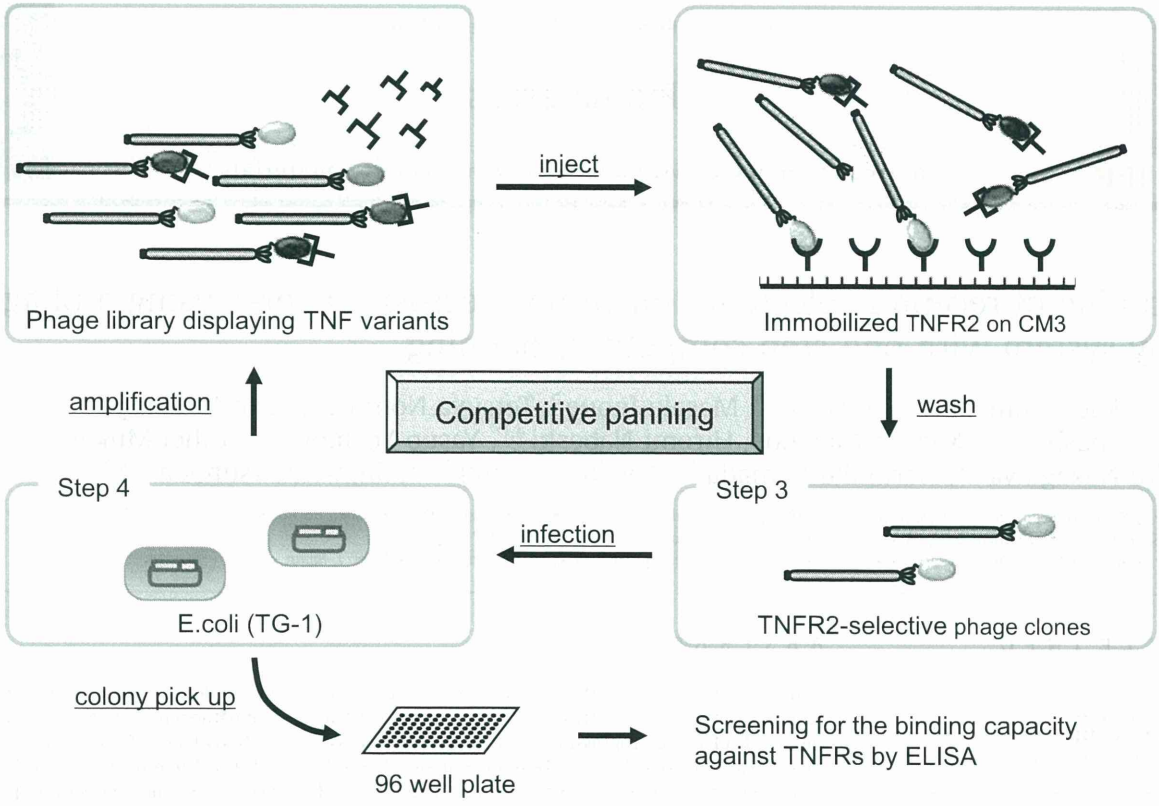

Fig. 1. Screening scheme for isolating TNFR2-selective TNF mutants using competitive panning. To concentrate TNFR2-selective mutant TNFs, phage libraries were pre-incubated with TNFR1 Fc chimera (TNFR1-Fc), and subsequent biopanning against the TNFR2 was carried out in the presence of TNFR1-Fc using the BIAcore biosensor. After several rounds of panning, phage clones were isolated and screened by ELISA.

for isolating TNFR2-selective mutants using the conventional panning method [23]. Out of the 500 clones, only 2 clones showed selectivity for TNFR2 binding that was 10-times higher than the wild-type TNF (wtTNF). Furthermore, bioactivities of these two TNFR2 selective TNF mutants were lower than that of wtTNF (<30%). To improve the screening efficacy, we optimized our phage display-based cytokine mutagenesis technology [25] with an unique competitive panning technique for identifying TNFR2-specific TNF mutants with higher affinity and bioactivity. In this competitive panning technique, phage libraries were pre-incubated with TNFR1 Fc chimera (TNFR1-Fc), and subsequent biopanning against the TNFR2 was carried out in the presence of TNFR1-Fc using the BIAcore biosensor. Since TNFR1-binding clones could not bind to TNFR2 due to steric hindrance, TNF mutants binding only to TNFR2 were selectively enriched with high efficiency. Using this optimized competitive panning technique, we have identified TNFR2-selective TNF mutants with full bioactivity via TNFR2.

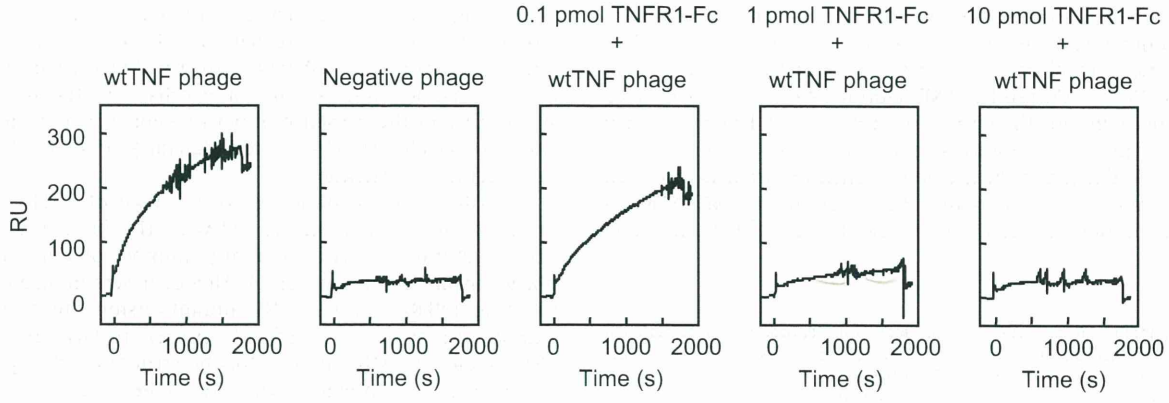

Fig. 2. Optimization of competitive panning using BIAcore biosensor. 0.1 pmol, 1 pmol or 10 pmol of human TNFR1-Fc was mixed with 1×10^{10} CFU phages displaying wtTNF for 2 h at 4 °C, and the mixture was passed over the TNFR2-immobilized CM3 sensor chip and real-time biomolecular interaction analyses were performed with BIAcore biosensor. Anti-CD25 single chain Fv-displaying phage was used as a negative control.

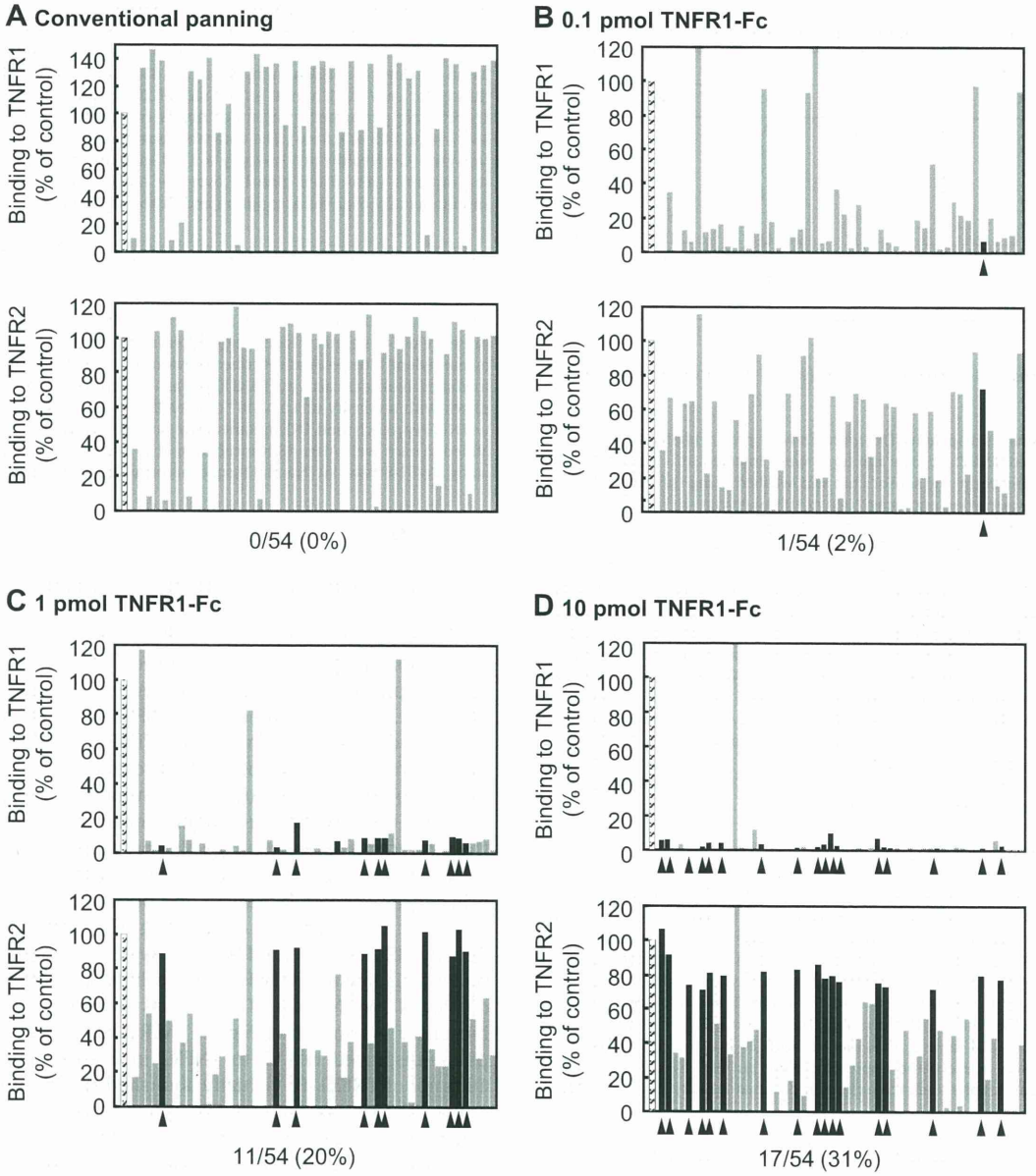

Fig. 3. Determination of relative affinities of mutant TNFs for TNFR1 or TNFR2 by capture ELISA. *E. coli* supernatant containing a TNF mutant (gray bar) from each panning conditions, in which phages were premixed with (A) none, (B) 0.1 pmol, (C) 1 pmol and (D) 10 pmol of TNFR1-Fc, were applied to the TNFR1-Fc or TNFR2-Fc immobilized plate and detected with biotinylated polyclonal anti-TNF antibody. wtTNF was used as a positive control (hatched bar). Affinities of TNFR2-selective clones (black bar) for TNFR2 was more than 70% of that of the wtTNF, and that for TNFR1 was less than 30% of that of the wtTNF.

2. Materials and methods

2.1. Cells

HEp-2 cells, a human fibroblast cell line, were provided by Cell Resource Center for Biomedical Research (Tohoku University, Sendai, Japan) and were maintained in RPMI 1640 (Sigma–Aldrich Japan, Tokyo, Japan) supplemented with 10% bovine fetal serum (FBS) 1 mM sodium pyruvate, 50 mM 2-mercaptoethanol, and antibiotics. hTNFR2/mFas-PA cells are preadipocytes derived from TNFR1$^{-/-}$R2$^{-/-}$ mice expressing a chimeric receptor, the extracellular and transmembrane domain of human TNFR2, and intracellular domain of mouse Fas; these cells were cultured in RPMI 1640 supplemented with 10% FBS, 5 μg/ml Blasticidin S HCl (Invitrogen, Carlsbad, CA), and antibiotics [26].

2.2. Library construction

Protocol for the construction of phage-display library displaying structural mutants of human TNF has been described previously [23]. In brief, multiple-mutations were introduced into the wtTNF gene by PCR to randomly replace the codons of 6 amino acid residues at positions 29, 31, 32, 145, 146 and 147, respectively, of the TNF protein. The PCR product was digested with the restriction enzymes Hind III and Not I, and ligated into the Hind III/Not I digested pY03′ phagemid vector for displaying the TNF mutants on the phage surface as g3p-fusion proteins.

2.3. Optimization of competitive panning using BIAcore biosensor

Human TNFR2-Fc (R&D systems, Minneapolis, MN) was diluted to 50 μg/ml in 10 mM sodium acetate buffer (pH 4.5) and immobilized onto a CM3 sensor chip using an amine coupling kit (GE Healthcare, UK), which resulted in an increase of 5000–6000 resonance units (RU). 0.1 pmol, 1 pmol or 10 pmol of human TNFR1-Fc (R&D systems) was mixed with 100 μl of wtTNF-displaying phage (1×10^{11} CFU/ml) for 2 h at 4 °C, and the mixture was passed over the TNFR2-immobilized CM3 sensor chip at a flow rate of 3 μl/min. The binding kinetics of the mixtures to TNFR2-Fc were analyzed by BIAcore 2000 (GE Healthcare).

Table 1
Amino acid sequences of wtTNF and TNFR2-selective TNF mutants.

Clone	Residue position					
	29	31	32	145	146	147
wtTNF	L	R	R	A	E	S
R2–6	L	R	R	H	E	D
R2–7	V	R	R	D	D	D
R2–8	L	R	R	N	D	D
R2–9	L	R	R	T	S	D
R2–10	L	R	R	Q	D	D
R2–11	L	R	R	T	D	D
R2–12	L	R	R	D	G	D
R2–13	L	R	R	D	E	D

2.4. Selection of phage displaying TNFR2-selective TNF mutants by competitive panning

1×10^{10} CFU phages displaying TNF mutants were pre-incubated for 2 h at 4 °C, with serially diluted TNFR1-Fc. The mixtures were injected at 3 μl/min over the sensor chip. After injection, the sensor chip was washed using the rinse command for 3 min. Elution was carried out using 20 μl of 10 mM glycine-HCl (pH 2.0) and the eluted phage was neutralized with 1 M Tris–HCl (pH 6.9). The recovered phages were amplified by infection of E. coli strain TG1 (Stratagene, La Jolla, CA), which allow read-through of the amber stop codon located between the TNF and g3p sequences of pY03′ phagemid vector. These steps were repeated twice. After final round of panning, the phage mixture was used to infect E. coli and plated on LB agar/ampicillin plates. Single clones of transfected TG1 were randomly picked from the plate and each colony was grown in 2-YT medium with ampicillin (100 μg/ml) and glucose (2% w/v) at 37 °C until the OD_{600} of the culture medium reached 0.4. Each culture was centrifuged, the supernatants were removed, and fresh 2-YT media with ampicillin (100 μg/ml) was added to each E. coli pellet. After incubation for 6 h at 37 °C supernatants were collected and used to determine affinity for TNFRs by capture ELISA as described previously [24]. After the procedure, the phagemid vectors were sequenced using a Big Dye Terminator v3.1 kit and ABI PRISM 3100 (Applied Biosystems Ltd., Pleasanton, CA).

2.5. Expression and purification of TNF mutants

Preparation of purified recombinant protein was described previously [25]. In brief, TNF mutants recombined into pYas1 vector, under the control of T7 promoter, were produced in E. coli (BL21λDE3). Mutant TNFs recovered from inclusion body, which were washed in Triton X-100 and solubilized in 6 M guanidine-HCl, 0.1 M Tris–HCl, pH 8.0, and 2 mM EDTA. Solubilized protein was adjusted to 10 mg/ml and was reduced with 10 mg/ml dithioerythritol for 4 h at RT and refolded by 100-fold dilution in a refolding buffer (100 mM Tris–HCl, 2 mM EDTA, 1 M arginine, and oxidized glutathione (551 mg/L)). After dialysis with 20 mM Tris–HCl, pH 7.4, containing 100 mM urea, active trimeric proteins were purified by Q-Sepharose (GE Healthcare)chromatography and size-exclusion chromatography (Superose 12; GE Healthcare).

2.6. Analysis of binding kinetics using surface plasmon resonance (SPR)

The binding kinetics of the wtTNF and TNF mutants were analyzed by the SPR technique (BIAcore 2000; GE Healthcare). TNFR1-Fc or TNFR2-Fc were separately immobilized on to CM5 sensor chip, resulting in an increase of 3000–3500 RU. During the association phase, wtTNF or TNF mutants diluted in running buffer (HBS-EP) at 156.8, 52.3, 17.4, 5.8 or 1.9 nM were passed over the immobilized TNFR2 for 2 min at a flow rate of 20 μl/min. During the dissociation phase, HBS-EP was run over the sensor chip for 1 min at a flow rate of 20 μl/min. The SPR measurements for TNFR1 were performed using much higher concentrations of TNF mutants (392.1, 130.7, 43.6, 14.5 or 4.8 nM). The data were analyzed globally with BIAevaluation 3.1 software (GE Healthcare) to apply a 1:1 Langmuir binding model. The obtained sensorgrams were fitted globally over the range of injected concentrations and simultaneously over the association and dissociation phages.

2.7. In vitro assessment of bioactivity via TNFR1 or TNFR2 with TNF mutants

HEp-2 cells were seeded at 4×10^4 cells/well in 96-well plates and incubated for 18 h with serially diluted wtTNF (Peprotech, Rocky Hill, NJ) or TNF mutants in the presence of 50 mg/ml cycloheximide. After incubation, cell survival was determined by methylene blue assay as described previously [25]. In the case of analyzing TNFR2-mediated biological activity, hTNFR2/mFas-PA were seeded on 96-well micro titer plates with a density of 1.5×10^4 cells/well in culture medium. Serial dilutions of wtTNF (Peprotech) and TNF mutants were prepared with 1 μg/ml cycloheximide and added to each well. After 48 h-incubation at 37 °C, the cell viabilities were analyzed using a WST-8 assay kit (Nacalai Tesque) according to the manufacturer's instructions.

3. Results

3.1. Optimization of one-step competitive panning protocol

To improve identifying TNFR2-selective TNF mutants with better bioactivity, we have introduced a step to remove the TNFR1-binding phages from the library by competitive panning using TNFR1-Fc. We postulated that TNFR1-binding clones could be eliminated when panning for the TNFR2-binding clones is performed in the presence of TNFR1 protein (see Fig. 1). Although an immunoplate or immunotube is commonly used for the panning [27–29], these techniques cannot make real-time observation of the interaction between phage library and receptor, and are difficult to automate and control the precise settings. Therefore, we first utilized the BIAcore biosensor and optimized the concentration of TNFR1-Fc required for eliminating the TNFR1-binding clones. Serially diluted human TNFR1-Fc was mixed with 1×10^{10} CFU phages displaying wtTNF, and the binding avidity of the phage-displayed wtTNF for TNFR2 was assessed using a BIAcore biosensor. As shown in Fig. 2, TNFR1-Fc inhibited the binding of phage-displayed wtTNF to TNFR2 in a dose-dependent manner. 10 pmol of TNFR1-Fc virtually abolished the binding of wtTNF not only to TNFR2 (last panel in Fig. 2) but also the binding of wtTNF to TNFR1 (data not shown). These results clearly suggest that 10 pmol of TNFR1-Fc would be sufficient for competitively subtract unwanted TNFR1-binding phage clones from a phage library displaying structural TNF mutants.

Table 2
Biding kinetics of TNFs to TNFR1 and TNFR2.

	TNFR1				TNFR2			
	k_{on}[a] (10^6 $M^{-1}s^{-1}$)	k_{off}[b] (10^{-4} s^{-1})	K_D[c] (10^{-10} M)	Relative[d] (%)	k_{on}[a] (10^6 $M^{-1}s^{-1}$)	k_{off}[b] (10^{-4} s^{-1})	K_D[c] (10^{-10} M)	Relative[d] (%)
wtTNF	0.45	1.3	2.9	100.0	2.0	12.1	6.1	100.0
R2–6	0.79	54.5	68.8	4.2	3.2	7.8	2.4	251.4
R2–7	0.44	116.0	262.0	1.1	2.1	7.4	3.6	169.7
R2–8	1.22	50.3	41.1	7.1	3.1	6.6	2.1	291.0
R2–9	1.19	50.1	42.3	6.9	3.8	12.6	3.3	185.2
R2–10	0.67	43.9	63.7	4.6	2.2	5.3	2.4	253.5
R2–11	0.81	87.5	108.	2.7	2.3	5.4	2.3	264.5
R2–12	1.36	98.8	72.6	4.0	4.1	10.6	2.6	235.0
R2–13	0.97	104.0	107.0	2.7	2.9	8.2	2.9	212.2

Kinetic parameters for each TNF were calculated from the respective sensorgram by BIAevaluation 3.1software, and taking into consideration that the TNF binds as a trimer.
[a] k_{on} is the association kinetic constant.
[b] k_{off} is the dissociation kinetic constant.
[c] K_D is the equilibrium dissociation constant ($K_D = k_{off}/k_{on}$).
[d] Relative values were calculated from the K_D (wtTNF)/K_D (TNF mutants) × 100.

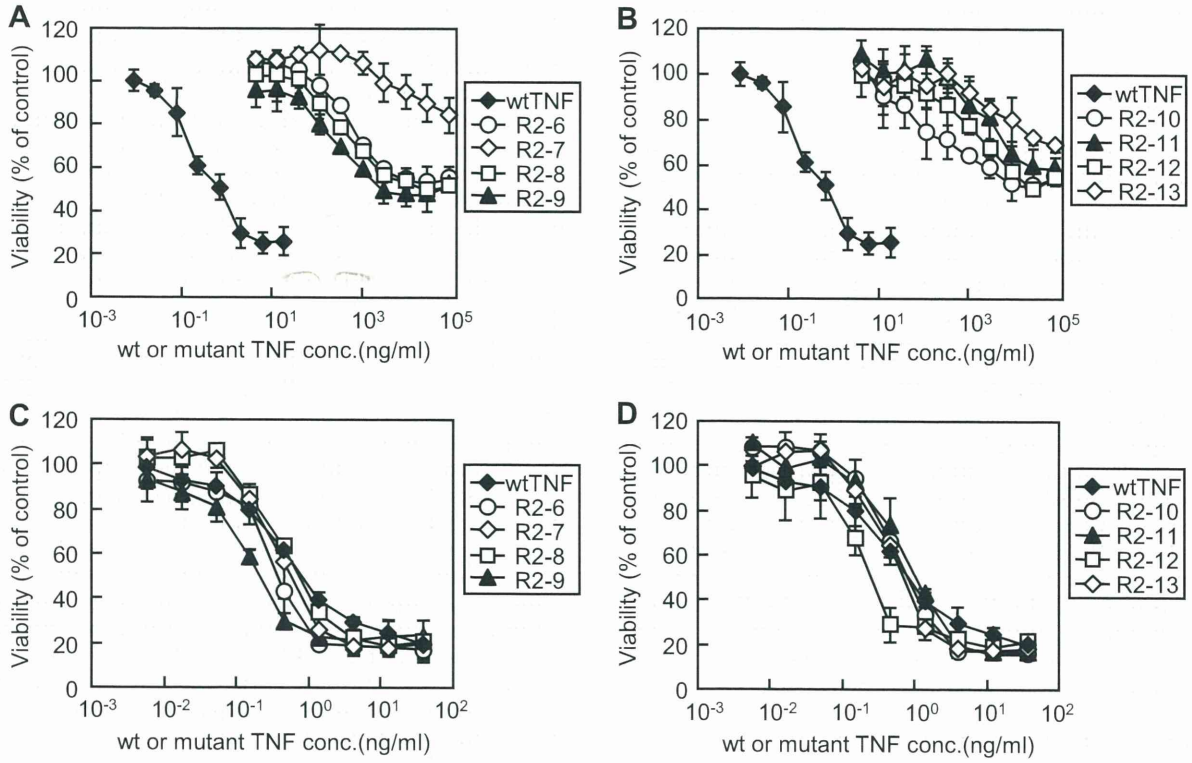

Fig. 4. In vitro bioactivity assay of TNF mutants via TNFR1 or TNFR2. The bioactivity of mutant TNFs via TNFR1 or TNFR2 were measured by cytotoxicity assay against HEp-2 cells (A and B) or hTNFR2/mFas-PA (C and D), respectively. Each point represents the mean ± S.D. of triplicate measurements.

3.2. Selection of TNFR2-selective TNF mutants by one-step competitive panning

To concentrate TNFR2-selective mutant TNFs, the TNF structural mutant displaying phage library was subjected to two rounds of conventional panning or competitive panning against TNFR2 using the BIAcore biosensor. After the second round of panning, *Escherichia coli* (TG1) supernatants of 54 randomly picked clones from each panning procedure were further screened by capture ELISA to analyze their binding specificities for each TNFR (Fig. 3). Consequently, we obtained numerous clones with high-affinity for TNFR2 under all panning conditions. Binding avidities of these clones for TNFR1 tended to decrease depending on the concentration of TNFR1-Fc used for premixing. However, binding avidity of a TNFR2-selective clone, which binds only to TNFR2 (Fig. 3, black bar), tended to increase depending on the concentration of TNFR1-Fc used for premixing. Almost all clones obtained from the conventional and competitive panning with 0.1 pmol of TNFR1-Fc (Fig. 3A and B, respectively) bound to TNFR1, and the panning efficiency for isolating the TNFR2-selective TNF mutants was <2%. In contrast, clones obtained from the subtracted panning with 1 or 10 pmol of TNFR1-Fc (Fig. 3C and D, respectively) contained many TNFR2-selective TNF mutants (>20%). From these panned clones, we eventually identified eight candidate agonists that selectively and strongly bound to the TNFR2. Amino acid sequences of these eight candidate TNFR2-selective TNF mutants are shown in Table 1. TNFR2-slective mutants were mutated near residue 145 and

Table 3
In vitro bioactivities of TNF mutants via TNFR1 or TNFR2.

	TNFR1[a]		TNFR2[b]		TNFR2/TNFR1[e]
	EC50[c] (ng/ml)	Relative Activity[d] (%)	EC50[c] (ng/ml)	Relative activity[d] (%)	
wtTNF	0.6	100	0.56	100	1.0
R2–6	8.1×10^{3}	7.3×10^{-3}	0.39	144	2.0×10^{4}
R2–7	$>1.0 \times 10^{5}$	$<6.0 \times 10^{-4}$	0.51	110	1.8×10^{5}
R2–8	4.6×10^{3}	1.2×10^{-2}	0.67	84	7.0×10^{3}
R2–9	2.1×10^{3}	2.8×10^{-2}	0.21	267	9.5×10^{3}
R2–10	1.1×10^{4}	5.4×10^{-3}	0.72	78	1.4×10^{4}
R2–11	6.7×10^{4}	8.9×10^{-4}	0.95	59	6.6×10^{4}
R2–12	2.6×10^{4}	2.2×10^{-3}	0.23	243	1.1×10^{5}
R2–13	$>1.0 \times 10^{5}$	$<6.0 \times 10^{-4}$	0.63	89	1.5×10^{5}

[a] Bioactivities of the wtTNF and TNF mutants via TNFR1 were measured by determining the TNF-induced cytotoxicity in HEp-2 cells.
[b] Bioactivities of the wtTNF and TNF mutants via TNFR2 were measured by determining the TNF-induced cytotoxicity in hTNFR2/mFas-PA.
[c] Experimental data were analyzed by a logistic regression model to calculate the mean effective concentration (EC50).
[d] Relative activities were calculated from the EC50 (wtTNF)/EC50 (TNF mutants).
[e] Selectivity for TNFR2 was calculated from the ratio of the relative activity (via TNFR2)/relative activity (via TNFR1).

conserved near residue 30. These findings indicate that the amino acid residues near position 30 are an essential for TNFR2 binding.

3.3. Binding kinetics of TNFR2-selective TNF mutants

To investigate the properties of eight TNFR2-selective TNF mutants in detail, we prepared recombinant protein using the previously described methods [30,31]. TNF mutants expressed as an inclusion body in *E. coli* (BL21λDE3) were denatured and refolded. Then, active TNF mutants were purified by ion–exchange and gel–filtration chromatography. TNF mutant purity was greater than 90% in sodium dodecyl sulfate–polyacrylamide gel electrophoresis, and all mutants were confirmed to form homotrimers in the same manner as the wtTNF by gel-filtration analysis (data not shown). To analyze the binding properties of these TNFR2-selective TNF mutants, we determined their binding dissociation constants (kinetic on- and off-rates) for TNFR1 and TNFR2, respectively, in detail using the surface plasmon resonance technique (Table 2). Our analysis showed that all eight mutant TNFs bound to the TNFR2 with high affinity; in contrast, they bound to the TNFR1 with greatly reduced affinity (typically between 1 and 7% of the wtTNF affinity). The dissociation constants (K_D) of these mutants for TNFR2 were between 2.1–3.6 $\times$ 10^{-10} M, and their relative affinities for TNFR2 were between 169 and 291% of that of the wtTNF. Thus, using the competitive panning technique we successfully obtained a large repertoire of TNFR2-selective TNF mutants with different binding parameters (on- and off-rates and dissociation constants).

3.4. Bioactivities of TNFR2-selective TNF mutants

To examine the bioactivity of these TNF mutants via TNFR1, we subsequently performed a cytotoxicity assay using HEp-2 cells (Fig. 4A and B). All TNF mutants (R2-6 ~ R2-13) showed almost no cytotoxicity, and the bioactivity was much lower than that of the wtTNF. Next, we evaluated the TNFR2-mediated activity of TNF mutants using the hTNFR2/mFas-PA, which were previously constructed in our laboratory [26]. The TNFR2-mediated bioactivities of these 8 mutant TNF proteins were at least same or higher than that of the wtTNF (Fig. 4C and D). As a negative control, we determined TNF cytotoxicity in parental TNFR1$^{-/-}$R2$^{-/-}$ preadipocytes and observed no wtTNF- or mutant TNF-mediated cell death (data not shown). Results of the cytotoxicity assay are summarized in Table 3. R2-7, the most highly TNFR2-selective mutant, exhibited 1.8 $\times$ 10^5 fold higher TNFR2-selectivity than that for the wild-type TNF.

4. Discussion

Recently, it was revealed that the two TNFRs worked together by crosstalk signaling, which suggested that the TNF-mediated signaling in the presence of both TNF receptors actually correlates with their physiological functions [32–34]. To understand the mechanism as well as to analyze the structure–function relationship of the TNFRs, several attempts were made in the past to create TNFR-specific mutant TNFs by conventional site-directed mutagenesis methods (such as Kunkel's method) [35–37]. However, these attempts were not very successful in yielding a desired TNF mutant having high receptor specificity and full bioactivity. For example, the TNFR2-binding affinity of the double mutant D143N-A145R was about 5–10 fold less than the wtTNF [38]. To overcome these problems, we applied phage-display technique and optimized panning method using the BIAcore biosensor (Fig. 1). Using an adequate amount of selective competitive inhibitor (>1 pmol TNFR1-Fc), this one-step competitive panning is ten times more efficient for screening TNFR2-selective TNF mutants, suggesting the competitive panning technology described here is a simple and effective screening method for fine-tuning TNF receptor-selectivity (Fig. 3). As a result of screening, we obtained successfully obtained TNFR2-selective TNF mutants with full bioactivity via TNFR2 (Table 3). Because of its high TNFR2-selectivity and full bioactivity, the TNF mutant R2-7 would help in elucidating the functional role of TNFR2.

One advantage of our phage-display-based technique is that it can be used to obtain the sequence information of many mutants [39,40]. It was previously shown by site-specific mutagenesis technique that mutations at positions 29, 31 and 32 (L29S, R31E and R32W) remarkably reduced the TNF's affinity for binding to TNFR2 [35,37,38]. For most of the TNFR2-selective TNF mutants, amino acids at positions 29, 31 and 32 were indeed identical (except for the R2-7 mutant which contained a conserved L to V substitution at position 29) to those of the wtTNF (Table 1), which is consistent with the previously reported idea that these three amino acids play critical roles in maintaining the binding between the TNF and TNFR2. The amino acid sequence at positions 145, 146 and 147 of the TNFR2-selective TNF mutants were, however, very different from those of the wtTNF. For example, the amino acid residue at position 145 of the TNF mutants R2-7, R2-12 and R2-13 contained an Asp residue in place of the Ala residue, and all of them showed high TNFR2 selectivity. Structural analysis and mutagenesis studies suggested that the loop containing the residues 145–147 is involved in the receptor binding [41–43]. Since Asp is a comparatively large residue, we speculated that this substitution could lead to a steric hindrance disrupting the interaction between the TNFR1 and TNFR2-selective mutants, which may be why they are less TNFR1-selective. However, why this replacement would increase the selectivity for TNFR2 is unclear at this moment. Currently, we are working on determining the structure of the TNF/TNFR2 complex by X-ray crystallography [44] so that structure–activity relationship studies could be initiated in the near future. Additionally, this structural information, in combination with bioinformatics technology, will be useful for designing TNFR-selective inhibitors (peptide mimics and chemical compounds).

5. Conclusions

In this study, we optimized our phage display-based screening using a unique competitive panning technique, which is ten times more efficient for screening TNFR2-selective TNF mutants compared to the conventional panning method. As a result of screening, we have succeeded in isolating several TNFR2-specific TNF mutants with high TNFR2 affinity and full bioactivity via TNFR2. Further analysis of the relationship between the structure and bioactivity of the TNF mutants would offer highly valuable and useful information regarding the TNF/TNFR biology. In conclusion, our fine-tuned competitive panning system is a simple and effective technology for isolating receptor-selective mutant proteins.

Acknowledgment

This study was supported in part by Grants-in-Aid for Scientific Research from the Ministry of Education, Culture, Sports, Science and Technology of Japan, and from the Japan Society for the Promotion of Science (JSPS). This study was also supported in part by Health Labour Sciences Research Grants from the Ministry of Health, Labor and Welfare of Japan, and by Health Sciences Research Grants for Research on Publicly Essential Drugs and Medical Devices from the Japan Health Sciences Foundation.

References

[1] Aggarwal BB. Signalling pathways of the TNF superfamily: a double-edged sword. Nat Rev Immunol 2003;3(9):745–56.
[2] Szlosarek PW, Balkwill FR. Tumour necrosis factor alpha: a potential target for the therapy of solid tumours. Lancet Oncol 2003;4(9):565–73.

[3] Aderka D, Engelmann H, Maor Y, Brakebusch C, Wallach D. Stabilization of the bioactivity of tumor necrosis factor by its soluble receptors. J Exp Med 1992; 175(2):323–9.
[4] Feldmann M, Maini RN. Lasker Clinical Medical Research Award. TNF defined as a therapeutic target for rheumatoid arthritis and other autoimmune diseases. Nat Med 2003;9(10):1245–50.
[5] Muto Y, Nouri-Aria KT, Meager A, Alexander GJ, Eddleston AL, Williams R. Enhanced tumour necrosis factor and interleukin-1 in fulminant hepatic failure. Lancet 1988;2(8602):72–4.
[6] Thorbecke GJ, Shah R, Leu CH, Kuruvilla AP, Hardison AM, Palladino MA. Involvement of endogenous tumor necrosis factor alpha and transforming growth factor beta during induction of collagen type II arthritis in mice. Proc Natl Acad Sci U S A 1992;89(16):7375–9.
[7] Williams RO, Feldmann M, Maini RN. Anti-tumor necrosis factor ameliorates joint disease in murine collagen-induced arthritis. Proc Natl Acad Sci U S A 1992;89(20):9784–8.
[8] Gomez-Reino JJ, Carmona L, Valverde VR, Mola EM, Montero MD. Treatment of rheumatoid arthritis with tumor necrosis factor inhibitors may predispose to significant increase in tuberculosis risk: a multicenter active-surveillance report. Arthritis Rheum 2003;48(8):2122–7.
[9] Lubel JS, Testro AG, Angus PW. Hepatitis B virus reactivation following immunosuppressive therapy: guidelines for prevention and management. Intern Med J 2007;37(10):705–12.
[10] Leist M, Gantner F, Jilg S, Wendel A. Activation of the 55 kDa TNF receptor is necessary and sufficient for TNF-induced liver failure, hepatocyte apoptosis, and nitrite release. J Immunol 1995;154(3):1307–16.
[11] Mori L, Iselin S, De Libero G, Lesslauer W. Attenuation of collagen-induced arthritis in 55-kDa TNF receptor type 1 (TNFR1)-IgG1-treated and TNFR1-deficient mice. J Immunol 1996;157(7):3178–82.
[12] Ware CF, Crowe PD, Vanarsdale TL, Andrews JL, Grayson MH, Jerzy R, et al. Tumor necrosis factor (TNF) receptor expression in T lymphocytes. Differential regulation of the type I TNF receptor during activation of resting and effector T cells. J Immunol 1991;147(12):4229–38.
[13] Irwin MW, Mak S, Mann DL, Qu R, Penninger JM, Yan A, et al. Tissue expression and immunolocalization of tumor necrosis factor-alpha in post-infarction dysfunctional myocardium. Circulation 1999;99(11):1492–8.
[14] Dopp JM, Sarafian TA, Spinella FM, Kahn MA, Shau H, de Vellis J. Expression of the p75 TNF receptor is linked to TNF-induced NFkappaB translocation and oxyradical neutralization in glial cells. Neurochem Res 2002;27(11):1535–42.
[15] Yang L, Lindholm K, Konishi Y, Li R, Shen Y. Target depletion of distinct tumor necrosis factor receptor subtypes reveals hippocampal neuron death and survival through different signal transduction pathways. J Neurosci 2002; 22(8):3025–32.
[16] Ban L, Zhang J, Wang L, Kuhtreiber W, Burger D, Faustman DL. Selective death of autoreactive T cells in human diabetes by TNF or TNF receptor 2 agonism. Proc Natl Acad Sci U S A 2008;105(36):13644–9.
[17] Monden Y, Kubota T, Inoue T, Tsutsumi T, Kawano S, Ide T, et al. Tumor necrosis factor-alpha is toxic via receptor 1 and protective via receptor 2 in a murine model of myocardial infarction. Am J Physiol Heart Circ Physiol 2007;293(1):H743–53.
[18] Wang M, Crisostomo PR, Markel TA, Wang Y, Meldrum DR. Mechanisms of sex differences in TNFR2-mediated cardioprotection. Circulation 2008;118(Suppl. 14):S38–45.
[19] Arnett HA, Mason J, Marino M, Suzuki K, Matsushima GK, Ting JP. TNF alpha promotes proliferation of oligodendrocyte progenitors and remyelination. Nat Neurosci 2001;4(11):1116–22.
[20] Faustman D, Davis M. TNF receptor 2 p.thway: drug target for autoimmune diseases. Nat Rev Drug Discov 2010;9(6):482–93.
[21] Fontaine V, Mohand-Said S, Hanoteau N, Fuchs C, Pfizenmaier K, Eisel U. Neurodegenerative and neuroprotective effects of tumor Necrosis factor (TNF) in retinal ischemia: opposite roles of TNF receptor 1 and TNF receptor 2. J Neurosci 2002;22(7). RC216.
[22] MacEwan DJ. TNF receptor subtype signalling: differences and cellular consequences. Cell Signal 2002;14(6):477–92.
[23] Mukai Y, Shibata H, Nakamura T, Yoshioka Y, Abe Y, Nomura T, et al. Structure-function relationship of tumor necrosis factor (TNF) and its receptor interaction based on 3D structural analysis of a fully active TNFR1-selective TNF mutant. J Mol Biol 2009;385(4):1221–9.
[24] Shibata H, Yoshioka Y, Ohkawa A, Minowa K, Mukai Y, Abe Y, et al. Creation and X-ray structure analysis of the tumor necrosis factor receptor-1-selective mutant of a tumor necrosis factor-alpha antagonist. J Biol Chem 2008;283(2):998–1007.
[25] Yamamoto Y, Tsutsumi Y, Yoshioka Y, Nishibata T, Kobayashi K, Okamoto T, et al. Site-specific PEGylation of a lysine-deficient TNF-alpha with full bioactivity. Nat Biotechnol 2003;21(5):546–52.
[26] Abe Y, Yoshikawa T, Kamada H, Shibata H, Nomura T, Minowa K, et al. Simple and highly sensitive assay system for TNFR2-mediated soluble- and transmembrane-TNF activity. J Immunol Methods 2008;335(1–2):71–8.
[27] Schwarz M, Rottgen P, Takada Y, Le Gall F, Knackmuss S, Bassler N, et al. Single-chain antibodies for the conformation-specific blockade of activated platelet integrin alphaIIbbeta3 designed by subtractive selection from naive human phage libraries. Faseb J 2004;18(14):1704–6.
[28] Popkov M, Rader C, Barbas 3rd CF. Isolation of human prostate cancer cell reactive antibodies using phage display technology. J Immunol Methods 2004; 291(1–2):137–51.
[29] Eisenhardt SU, Schwarz M, Bassler N, Peter K. Subtractive single-chain antibody (scFv) phage-display: tailoring phage-display for high specificity against function-specific conformations of cell membrane molecules. Nat Protoc 2007;2(12):3063–73.
[30] Shibata H, Yoshioka Y, Abe Y, Ohkawa A, Nomura T, Minowa K, et al. The treatment of established murine collagen-induced arthritis with a TNFR1-selective antagonistic mutant TNF. Biomaterials 2009;30(34):6638–47.
[31] Shibata H, Yoshioka Y, Ikemizu S, Kobayashi K, Yamamoto Y, Mukai Y, et al. Functionalization of tumor necrosis factor-alpha using phage display technique and PEGylation improves its antitumor therapeutic window. Clin Cancer Res 2004;10(24):8293–300.
[32] Wajant H, Pfizenmaier K, Scheurich P. Tumor necrosis factor signaling. Cell Death Differ 2003;10(1):45–65.
[33] Weiss T, Grell M, Siemienski K, Muhlenbeck F, Durkop H, Pfizenmaier K, et al. TNFR80-dependent enhancement of TNFR60-induced cell death is mediated by TNFR-associated factor 2 and is specific for TNFR60. J Immunol 1998; 161(6):3136–42.
[34] Fotin-Mleczek M, Henkler F, Samel D, Reichwein M, Hausser A, Parmryd I, et al. Apoptotic crosstalk of TNF receptors: TNF-R2-induces depletion of TRAF2 and IAP proteins and accelerates TNF-R1-dependent activation of caspase-8. J Cell Sci 2002;115(Pt. 13):2757–70.
[35] Yamagishi J, Kawashima H, Matsuo N, Ohue M, Yamayoshi M, Fukui T, et al. Mutational analysis of structure–activity relationships in human tumor necrosis factor-alpha. Protein Eng 1990;3(8):713–9.
[36] Barbara JA, Smith WB, Gamble JR, Van Ostade X, Vandenabeele P, Tavernier J, et al. Dissociation of TNF-alpha cytotoxic and proinflammatory activities by p55 receptor- and p75 receptor-selective TNF-alpha mutants. Embo J 1994; 13(4):843–50.
[37] Van Ostade X, Vandenabeele P, Everaerdt B, Loetscher H, Gentz R, Brockhaus M, et al. Human TNF mutants with selective activity on the p55 receptor. Nature 1993;361(6409):266–9.
[38] Loetscher H, Stueber D, Banner D, Mackay F, Lesslauer W. Human tumor necrosis factor alpha (TNF alpha) mutants with exclusive specificity for the 55-kDa or 75-kDa TNF receptors. J Biol Chem 1993;268(35):26350–7.
[39] Abe Y, Nomura T, Yoshioka Y, Kamada H, Tsunoda S, Tsutsumi Y. Anti-inflammatory effects of a Novel TNFR1-selective antagonistic TNF mutant on established murine collagen-induced arthritis. Adv Exp Med Biol 2011;691:493–500.
[40] Yoshioka Y, Watanabe H, Morishige T, Yao X, Ikemizu S, Nagao C, et al. Creation of lysine-deficient mutant lymphotoxin-alpha with receptor selectivity by using a phage display system. Biomaterials 2010;31(7):1935–43.
[41] Eck MJ, Sprang SR. The structure of tumor necrosis factor-alpha at 2.6 A resolution. Implications for receptor binding. J Biol Chem 1989;264(29):17595–605.
[42] Van Ostade X, Tavernier J, Fiers W. Structure–activity studies of human tumour necrosis factors. Protein Eng 1994;7(1):5–22.
[43] Idriss HT, Naismith JH. TNF alpha and the TNF receptor superfamily: structure-function relationship(s). Microsc Res Tech 2000;50(3):184–95.
[44] Mukai Y, Nakamura T, Yoshikawa M, Yoshioka Y, Tsunoda S, Nakagawa S, et al. Solution of the structure of the TNF-TNFR2 complex. Sci Signal 2010;3(148). ra83.

Laboratory of Bio-Functional Molecular Chemistry[1], Laboratory of Toxicology and Safety Science[2], Graduate School of Pharmaceutical Sciences[3], Osaka University, Suita; Laboratory of Biopharmaceutical Research (Pharmaceutical Proteomics), National Institute of Biomedical Innovation, Ibaraki, Osaka, Japan

Effect of surface charge on nano-sized silica particles-induced liver injury

K. ISODA[1], T. HASEZAKI[1], M. KONDOH[1], Y. TSUTSUMI[2,3], K. YAGI[1]

Received October 5, 2010, accepted November 11, 2010

Dr Kiyohito Yagi, Laboratory of Bio-Functional Molecular Chemistry, Graduate School of Pharmaceutical Sciences, Osaka University, Suita, Osaka 565-0871, Japan
yagi@phs.osaka-u.ac.jp

Pharmazie 66: 278–281 (2011) *doi: 10.1691/ph.2011.0808*

Nanomaterials are used frequently in microelectronics, cosmetics and sunscreen, and research for the development of nanomaterial-based drug delivery systems is promising. We previously reported that the intravenous administration of unmodified silica particles with a diameter of 70 nm (SP70) caused hepatic injury. Here, we examined the acute hepatic toxicity of SP70 modified with amino group (SP70-N) or carboxyl group (SP70-C). When administered intravenously into mice, SP70-N and SP70-C dose-dependently increased the serum level of alanine aminotransferase (ALT). However, the toxicity levels of surface charge-modified silica particles were much less weaker than the level of unmodified particles. When SP70 was repeatedly administered at 40 mg/kg twice a week for 4 weeks into mice, the hydroxyproline content of the liver significantly increased. Azan staining of the liver section indicated the extensive fibrosis. To the contrary, the repeated administration of SP70-N or SP70-C at 60 mg/kg twice a week for 4 weeks into mice did not cause the hepatic fibrosis. These findings suggest that the surface charge of nanomaterials could change their toxicity.

1. Introduction

Recently, the scientific, medical, and technical applications of nanomaterials have greatly increased. Nanomaterials are frequently used in microelectronics, cosmetics and sunscreen, and their potential use in drug-delivery systems is being investigated (Dobson 2006). Nanomaterials have unique physicochemical qualities as compared to micromaterials in regard to size, surface structure, solubility, and aggregation. Thus, the reduction in particle size from the micro- to nanoscale is beneficial for many industrial and scientific applications. However, nanomaterials have potential toxicity that is not found in micromaterials, and it is, therefore, essential to understand the biological activity and potential toxicity of nanomaterials (Warheit et al. 2008).

The physical properties of nanomaterials are changed by the modification of their surface charge, which extends their possible applications. For example, charge-modified dendrimers are expected to have applications in drug-delivery systems. The physical properties and the toxicity of carbon nanotubes change based on the surface charge (Smith et al. 2009), as do the pharmacokinetics of liposomes. Future research will undoubtedly lead to expanded applications of surface-modified nanomaterials, however, little has been reported on their toxicity.

Silica nanoparticles have been applied to diagnostic measures and drug delivery methods. Intraperitoneal administration of silica nanoparticles results in the biodistribution of the nanoparticles to diverse organs, such as the liver, kidney, spleen and lung (Kim et al., 2006). We previously found that nano-size silica particles with a diameter of 70 nm caused liver injury, while micro-size particles with a diameter of 300 or 1000 nm did not (Nishimori et al. 2009a, b). In the present study, we examined the hepatic toxicity of surface charge-modified silica nanoparticles.

2. Investigations, results and discussion

The surface modification technology has been developed in the field of nanotechnology (Schiestel et al. 2004), and many nanomaterials with new functions will be produced for cosmetics and medicinal use. Thus, it should be important to investigate the effect of surface charge of nanomaterials on living body.

We initially examined the acute toxicity of 70-nm diameter silica nanoparticles (SP70) modified with amino group (SP70-N) or carboxyl group (SP70-C) at the maximal dose of 100 mg/kg. Intravenous injection of 50 mg/kg of unmodified SP70 was lethal in mice (Fig. 1A). The acute liver toxicity of SP70-N and SP70-C increased in a dose-dependent manner (Fig. 1B, C). Intravenous injection of SP70-C was lethal in all mice at 100 mg/kg and was often lethal at 80 and 60 mg/kg. SP70-C was more toxic than SP70-N. We examined the hepatic injury caused by 40 mg/kg of unmodified SP70 and 60 mg/kg of modified SP70 (SP70-C and SP70-N). The hematoxylin-eosin staining of liver tissue from mice injected with the silica nanoparticles is shown in Fig. 2A–D. The liver injury caused by SP70 was more extensive than that caused by SP70-C and SP70-N. Significant increase in the levels of BUN, a biochemical marker of kidney injury, was not observed in mice that received the nanoparticles (Fig. 3). The less amount of unmodified SP70 induced significant liver damage than the surface-modified silica particles. Thus, the

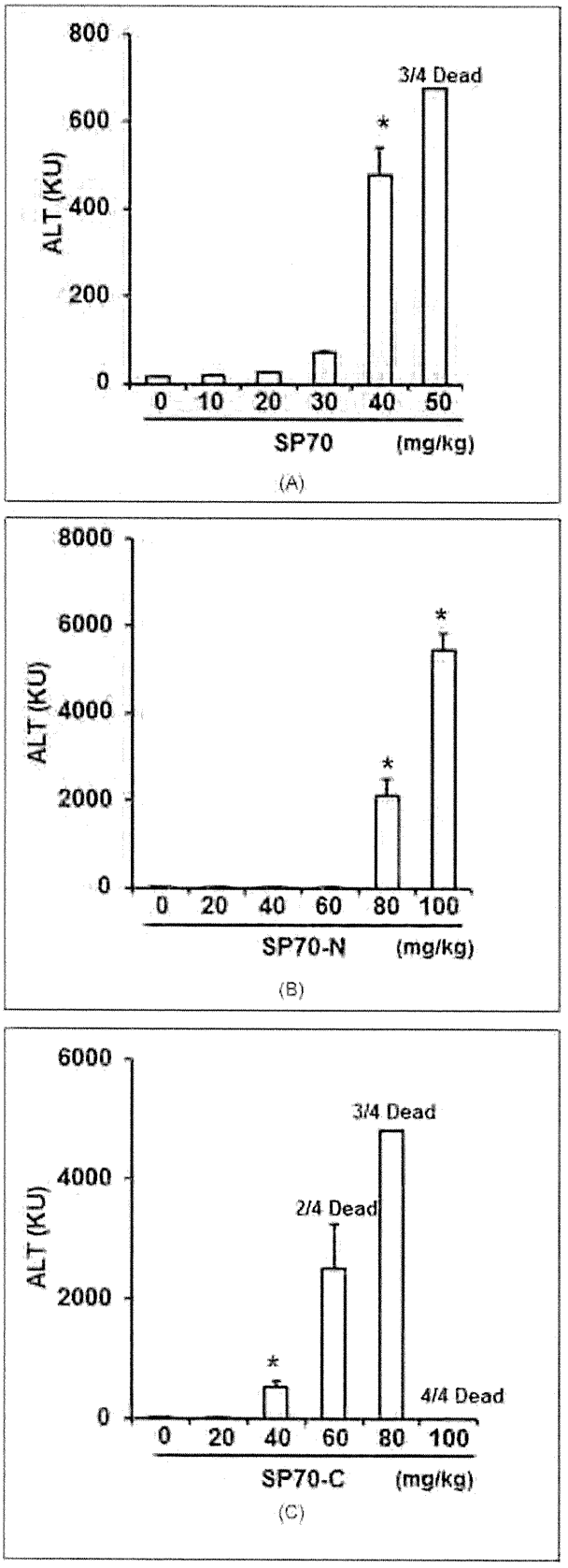

Fig. 1: Acute liver toxicity of SP70-N and SP70-C. SP70 (A), SP70-N (B) and SP70-C (C) were intravenously administered at the indicated doses. At 24 h after administration, blood was collected, and the resultant serum was used for the ALT assay. Data are means ± SEM (n = 4). *$p < 0.05$ as compared to the vehicle-treated group.

modification of the surface charge decreased the amount of acute hepatic injury caused by silica nanoparticles.

We then examined the chronic liver injury caused by 60 mg/kg of SP70-C or SP70-N as compared to 30 mg/kg of SP70. Nanoparticles were intravenously injected into mice twice a week for 4 weeks. We assessed the presence of liver fibrosis, because it is a symptom of chronic liver injury. We determined the hepatic hydroxyproline contents in the silica nanoparticle–treated mice (Fig. 4A). SP70, but not SP70-N or SP70-C, significantly increased the hepatic hydroxyproline content by 3.5-fold over the control value. Moreover, collagen, which accumulates in the fibrotic liver, was stained with Azan reagent, and blue-stained regions were observed in SP70-treated, but not SP70-C- and SP70-N-treated, liver sections (Fig. 4B-E). Thus, the chronic administration of SP70-C and SP70-N did not cause hepatic fibrosis in mice.

In this study we found that the surface modification of nanosilica particles with amino group and carboxyl group attenuated liver toxicity. We suspect that this decreased toxicity is due to a decrease in the amount of silica nanoparticles that accumulate in the liver. Oku et al. (1996) reported that the accumulation of liposomes in the liver changed depending on the surface charge of liposomes. Although we confirmed the presence of SP70-N, SP70-C and SP70 in the electron micrograph (data not shown), we were unable to compare the accumulative amounts in the liver. Therefore, an analysis of the accumulative amount of the silica nanoparticles in the liver is necessary in future studies.

The surface charge of nanoparticles might change the pharmacokinetics *in vivo*; for instance, the silica nanoparticles with a positive surface charge have increased paracellular permeability (Lin et al. 2007). Moreover, the phagocytosis of liposomes by hepatic Kupffer cells was promoted by a positive surface charge (Schiestel et al. 2004). We previously reported that the inhibition of phagocytosis by Kupffer cells increased the toxicity of nanosilica particles (Nishimori et al. 2009a). Therefore, it is thought that the nanoparticles with a positive surface charge have decreased hepatic toxicity due to increased phagocytosis by liver Kupffer cells.

This report is the first to indicate that altering the surface charge of nanomaterials changes their toxicity. Further studies based on these data will provide useful information regarding the safety of the nanomaterials.

3. Experimental

3.1. Materials

Silica particles with a diameter of 70 nm were obtained from Micromod Partikeltechnologie GmbH (Rostock, Germany). Silica particles with a diameter of 70 nm that were modified with the amino group or the carboxyl group were obtained from Micromod Partikeltechnologie GmbH (Rostock, Germany). The size distribution of the particles was analyzed using a Zetasizer (Sysmex Co., Kobe, Japan), and the mean diameters were 61.5 and 70.5 nm, respectively. The electric charge of the particles, also measured using the Zetasizer, was found to be –19.7 and –52.4 mV, respectively. The particles were spherical and nonporous and were stored at 25 mg/mL in an aqueous suspension. The suspensions were thoroughly dispersed by sonication before use and then diluted in ultrapure water. All reagents used were of research grade.

3.2. Animals

Eight-week-old BALB/c male mice were purchased from Shimizu Laboratory Supplies Co., Ltd. (Kyoto, Japan) and were maintained in a controlled environment (23 ± 1.5 °C; 12-h light/dark cycle) with access to standard rodent chow and water *ad libitum*. The mice were left to adapt to the new environment for 1 week before commencing with the experiment. Mice that received a single treatment of silica nanoparticles were anesthetized for sacrificing 24 h after intravenous injection. Mice in the frequent treatment group received intravenous administration of silica nanoparticles twice a week for 4 weeks. The experimental protocols conformed to the ethical guidelines of the Graduate School of Pharmaceutical Sciences, Osaka University.

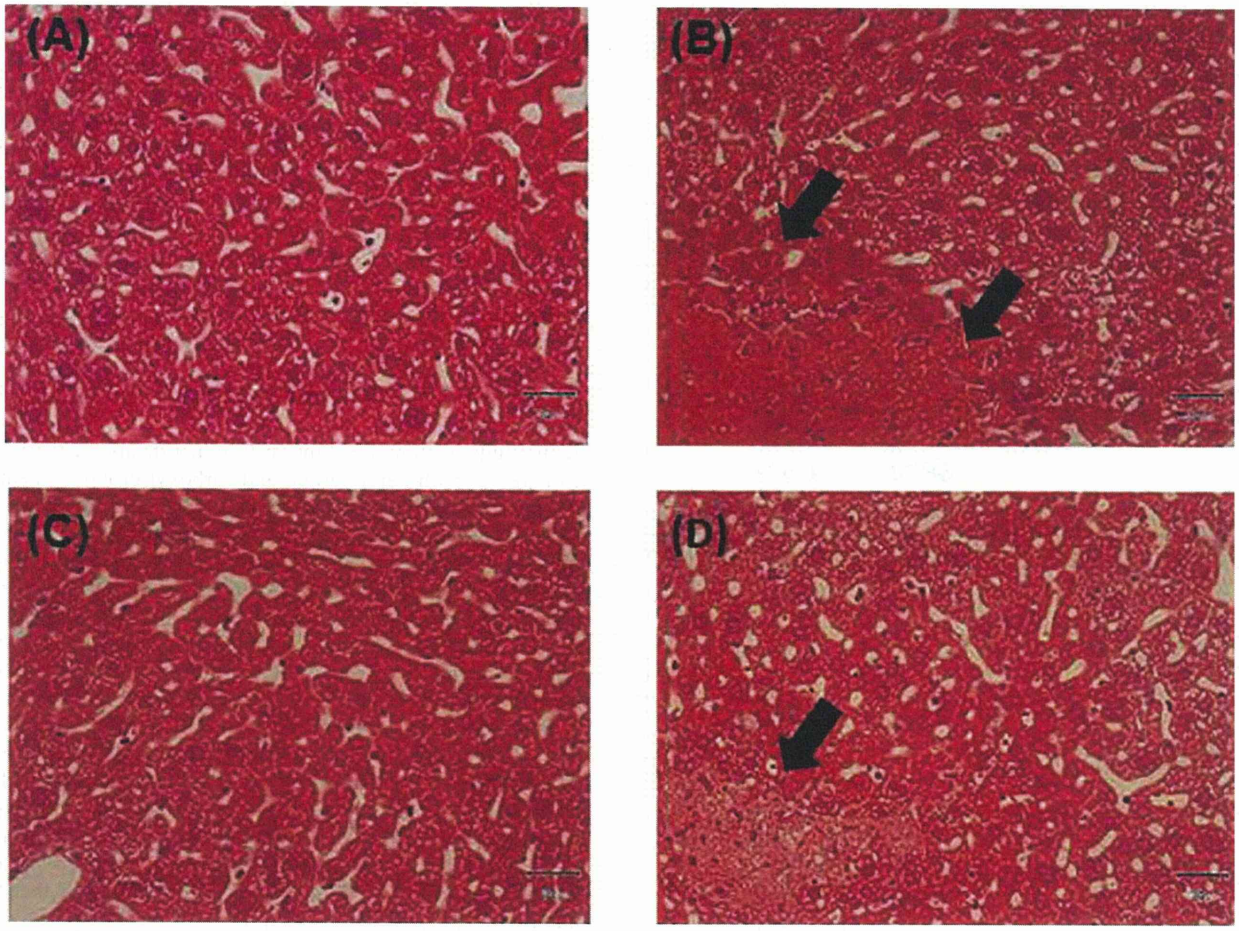

Fig. 2: Hematoxylin and eosin staining of the liver sections. Twenty-four h after administration, the liver was excised from the mice treated with vehicle (A), SP70 (B), SP70-N (C) or SP70-C (D) and fixed with 4% paraformaldehyde. Tissue sections were stained with hematoxylin and eosin and observed under a microscope. The arrows indicate areas of hepatic injury.

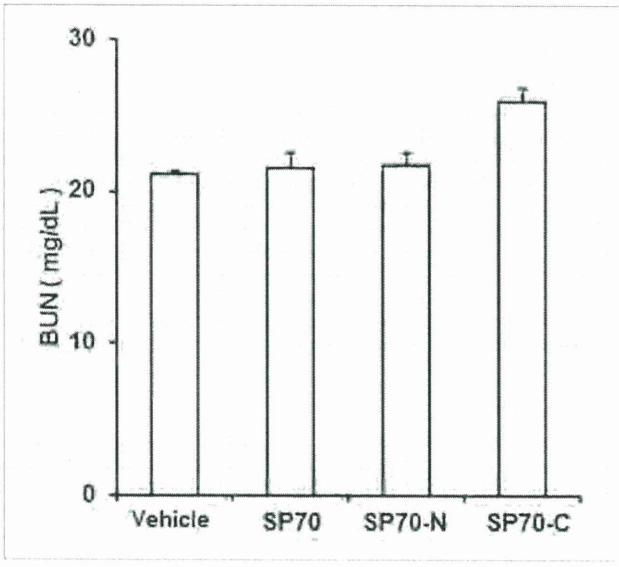

Fig. 3: Effect of SP70-N and SP70-C on kidney. SP70, SP70-N and SP70-C were intravenously administered at 40 mg/kg, 60 mg/kg, and 60 mg/kg, respectively. At 24 h after administration, blood was collected, and the resultant serum was used for the BUN assay with a commercially available kit. Data are means ± SEM (n = 4).

3.3. Biochemical analysis

Serum alanine aminotransferase (ALT) and blood urea nitrogen (BUN) were measured with commercially available kits according to the manufacturer's protocols (Wako Pure Chemical Industries, Osaka, Japan).

3.4. Histological analysis

The liver was excised and fixed with 4% paraformaldehyde. After sectioning, thin tissue sections of tissues were stained with hematoxylin and eosin for histological observation. Liver sections were stained with Azan-Mallory for observation of liver fibrosis.

3.5. Measurement of hydroxyproline content

Hepatic hydroxyproline (HYP) content was measured using Kivirikko's method (Kivirikko et al. 1967), with some modifications. Briefly, liver tissue (50 mg) was hydrolyzed in 6 mol/L HCl at 110 °C for 24 h in a glass test tube. After centrifugation at 3000 rpm for 10 min, 2 mL of the supernatant was neutralized with 8 N KOH. Two grams of KCl and 1 mL of 0.5 mol/L borate buffer were then added to the resultant solution, followed by incubation for 15 min at room temperature and a further incubation for 15 min at 0 °C. Freshly prepared chloramine-T solution was then added and the solution was incubated at 0 °C for 1 h, followed by the addition of 2 mL of 3.6 mol/L sodium thiosulfate. The samples were incubated at 120 °C for 30 min, and then 3 mL toluene was added with incubation for a further 20 min at room temperature. After centrifugation at 2000 rpm for 5 min, 2 mL of the supernatant was added to 0.8 mL of buffer containing Ehrlich's reagent and incubated for 30 min at room temperature. The samples were then transferred to a plastic tube and the absorbance was measured at 560 nm. Hydroxyproline content was expressed as micrograms of hydroxyproline per gram of liver.